

## Intermolecular potential energy surface and thermophysical properties of ethylene oxide

Johann-Philipp Crusius, Robert Hellmann, Egon Hassel, and Eckard Bich

Citation: *The Journal of Chemical Physics* **141**, 164322 (2014); doi: 10.1063/1.4899074

View online: <http://dx.doi.org/10.1063/1.4899074>

View Table of Contents: <http://scitation.aip.org/content/aip/journal/jcp/141/16?ver=pdfcov>

Published by the [AIP Publishing](#)

---

### Articles you may be interested in

[Ab initio potential energy surface for methane and carbon dioxide and application to vapor-liquid coexistence](#)  
*J. Chem. Phys.* **141**, 064303 (2014); 10.1063/1.4891983

[Ab initio ground state phenylacetylene–argon intermolecular potential energy surface and rovibrational spectrum](#)  
*J. Chem. Phys.* **137**, 074305 (2012); 10.1063/1.4742153

[Ab initio potential energy surface and intermolecular vibrations of the naphthalene–argon van der Waals complex](#)  
*J. Chem. Phys.* **134**, 064322 (2011); 10.1063/1.3555765

[Nitrous oxide dimer: A new potential energy surface and rovibrational spectrum of the nonpolar isomer](#)  
*J. Chem. Phys.* **133**, 134304 (2010); 10.1063/1.3494542

[The water–nitric oxide intermolecular potential–energy surface revisited](#)  
*J. Chem. Phys.* **130**, 104303 (2009); 10.1063/1.3079541

---



**2014 Special Topics**

PEROVSKITES

2D MATERIALS

MESOPOROUS MATERIALS

BIOMATERIALS/  
BIOELECTRONICS

METAL-ORGANIC  
FRAMEWORK  
MATERIALS

**AIP** | APL Materials

**Submit Today!**

# Intermolecular potential energy surface and thermophysical properties of ethylene oxide

Johann-Philipp Crusius,<sup>1,a)</sup> Robert Hellmann,<sup>2</sup> Egon Hassel,<sup>1</sup> and Eckard Bich<sup>2</sup>

<sup>1</sup>*Lehrstuhl für Technische Thermodynamik, Universität Rostock, 18059 Rostock, Germany*

<sup>2</sup>*Institut für Chemie, Universität Rostock, 18059 Rostock, Germany*

(Received 7 August 2014; accepted 10 October 2014; published online 29 October 2014; publisher error corrected 4 November 2014)

A six-dimensional potential energy hypersurface (PES) for two interacting rigid ethylene oxide ( $C_2H_4O$ ) molecules was determined from high-level quantum-chemical *ab initio* calculations. The counterpoise-corrected supermolecular approach at the MP2 and CCSD(T) levels of theory was utilized to determine interaction energies for 10178 configurations of two molecules. An analytical site-site potential function with 19 sites per ethylene oxide molecule was fitted to the interaction energies and fine tuned to agree with data for the second acoustic virial coefficient from accurate speed of sound measurements. The PES was validated by computing the second virial coefficient, shear viscosity, and thermal conductivity. The values of these properties are substantiated by the best experimental data as they tend to fall within the uncertainty intervals and also obey the experimental temperature functions, except for viscosity, where experimental data are insufficient. Due to the lack of reliable data, especially for the transport properties, our calculated values are currently the most accurate estimates for these properties of ethylene oxide. © 2014 AIP Publishing LLC. [<http://dx.doi.org/10.1063/1.4899074>]

## I. INTRODUCTION

The calculation of thermophysical properties of fluids based on molecular models is of great interest for use in industrial applications, while at the same time allowing for the validation of the calculation methods. Provided the theoretical models resemble the true nature of the intermolecular forces, the accuracy of the calculated fluid properties is on a par with experimental data. This allows for a better understanding of the microscopic processes and serves to supplement or even to substitute experimental data. This is especially useful for fluids where the available data are of low accuracy or nonexistent, especially at conditions that are difficult or dangerous to handle in an experiment.

Ethylene oxide (EtO) ranks under the top most produced organic chemicals in the world, with  $20 \times 10^6$  tons produced in 2009<sup>1</sup> and rising. It serves as a precursor for many important chemical and pharmaceutical compounds. Surprisingly, the available thermophysical data are very scarce and in dire need of improvement. The demand for precise thermophysical data for industrial processes is furthermore underlined by the fact that ethylene oxide was chosen as the substance of interest in the Fourth Industrial Fluid Properties Simulation Challenge in 2008.<sup>2</sup> The challenge's objective was to simulate a wide range of thermodynamic and transport properties for both the liquid and the vapor phase at 375 K. The challenge gave rise to several publications<sup>3-9</sup> on the computational simulation of ethylene oxide properties.

In this paper, we present a new *ab initio* potential energy hypersurface (PES) for two ethylene oxide molecules. We ap-

plied the counterpoise-corrected supermolecular approach to determine interaction energies at the MP2 and CCSD(T)<sup>10</sup> levels of theory for 10178 dimer configurations. To this end, we used basis sets of double-zeta and triple-zeta quality with additional bond functions located between the two monomers. The interaction energies were extrapolated to the complete basis set (CBS) limit using a flexible extrapolation scheme to allow for a fine tuning of the PES to second acoustic virial coefficients from accurate speed of sound measurements. We fitted an analytical 19-center site-site potential function with isotropic site-site interactions to the extrapolated interaction energies, fully optimizing the interaction parameters as well as the positions of the sites during the fit.

The new PES was validated by calculating several thermophysical properties of ethylene oxide gas. The second virial coefficients and second acoustic virial coefficients were evaluated using statistical thermodynamics. Quantum effects were incorporated by means of the quadratic Feynman-Hibbs (QFH) effective pair potential.<sup>11</sup> Shear viscosity and thermal conductivity in the dilute-gas limit were determined using the classical trajectory approach in conjunction with the kinetic theory of gases for rigid molecules.<sup>12-15</sup> We present accurate values for these properties of ethylene oxide vapor for a wide temperature range, thereby adding theoretically determined values to the little available experimental data and supplying reliable reference values for the future.

In Sec. II, we describe the development of the analytical potential function in detail. In Sec. III, we summarize the theory and the results for the second virial coefficients and second acoustic virial coefficients, and in Sec. IV we do the same for the transport properties. We give a summary and present our conclusions in Sec. V.

<sup>a)</sup>Electronic mail: johann-philipp.crusius@uni-rostock.de.

## II. INTERMOLECULAR POTENTIAL

### A. Monomer geometry

The intermolecular potential between two ethylene oxide molecules is a 36-dimensional hypersurface if all intramolecular degrees of freedom are considered explicitly. Such high dimensionality would require an unfeasible number of *ab initio* calculations to adequately sample the entire PES. If instead the monomers are assumed to be rigid rotors, the PES is only six-dimensional. Past experience for different small molecules shows that nevertheless a highly accurate intermolecular PES can be constructed when using the zero-point vibrationally averaged geometry for the rigid monomers, see, for example, Refs. 16–19.

The zero-point vibrationally averaged geometry for ethylene oxide was calculated in multiple steps fully *ab initio* at the CCSD(T) level of theory. First, the geometry was optimized with all electrons correlated using the cc-pwCV5Z basis set<sup>20</sup> to obtain the best possible equilibrium geometry. Then the difference between the zero-point vibrationally averaged geometry and the equilibrium geometry was calculated. For this purpose, the equilibrium geometry was determined at the cc-pVTZ basis set level applying the frozen-core approximation, followed by a cubic force-field calculation, which yielded the cc-pVTZ zero-point vibrationally averaged geometry. Finally, the differences in the bond lengths and bond angles between the vibrationally averaged and the equilibrium geometries at the cc-pVTZ level were added to the corresponding values of the cc-pwCV5Z equilibrium geometry determined in the first step. Thus, we obtained an approximation of the vibrationally averaged geometry at the cc-pwCV5Z level. This final geometry is consistent with data obtained from rovibrational spectroscopy<sup>21,22</sup> and was used for all further calculations. The geometry, bond lengths, and bond angles, including the spectroscopically determined values, can be found in the supplementary material.<sup>23</sup>

### B. *Ab initio* calculation of interaction energies

Each configuration of two rigid ethylene oxide molecules can be expressed as a function of the distance  $R$  between the centers of mass of the monomers and the five Euler-angles  $\theta_1$ ,  $\theta_2$ ,  $\psi_1$ ,  $\psi_2$ , and  $\phi$ , see the supplementary material<sup>23</sup> for details. Two sets of angular configurations were generated by varying all five angles between  $0^\circ$  and  $180^\circ$  in steps of  $45^\circ$  starting at  $0^\circ$  and  $22.5^\circ$ , respectively, which resulted in a total of 949 (405 for set one and 544 for set two) distinct angular configurations. Values higher than  $180^\circ$  for the angles are not needed due to symmetry. Eleven center of mass separations between 2.5 Å and 12.0 Å were considered for the first set of angles and further 11 separations between 2.75 Å and 15.0 Å for the second set, resulting in a total of 10439 EtO–EtO configurations of which 267 at small distances had to be discarded because either two atoms were too close to each other in these configurations or the quantum-mechanical computations failed due to near linear dependencies in the basis sets used. In a preliminary fit of the potential function six local minima, including the global minimum, were iden-

tified. Interaction energies for these six configurations were then also computed by quantum-mechanical means, which finally yielded a total of 10178 points. It should be noted that the preliminary PES showed good predictive behaviour with respect to the local minima in comparison with the actual values obtained from the quantum-mechanical calculations afterwards.

We have calculated the interaction energies  $V(R, \theta_1, \theta_2, \psi_1, \psi_2, \phi)$  for all 10178 configurations following the supermolecular approach including the full counterpoise correction<sup>24</sup> at the frozen-core MP2 level of theory applying the aug-cc-pVXZ basis sets<sup>25</sup> for  $X = 2$  and  $X = 3$ . The two basis sets were supplemented by a small *3s3p2d1f* set of bond functions positioned in the center of mass of the molecule pair. The exponents of the bond functions are 0.1, 0.3, and 0.9 for  $s$  and  $p$ , 0.25 and 0.75 for  $d$ , and 0.45 for  $f$ . The correlation parts of the interaction energies,  $V_{\text{MP2 corr}}$ , computed with the two basis sets, were extrapolated to the CBS limit using the two-point extrapolation scheme proposed by Halkier *et al.*,<sup>26</sup>

$$V_{\text{MP2 corr}}(X) = V_{\text{MP2 corr}}^{\text{CBS}} + \alpha X^{-\beta}, \quad (1)$$

where  $\beta = 3$ . The SCF energies were not extrapolated, as the differences between the results for the two basis sets are quite small already. Hence, we used the SCF interaction energies from the aug-cc-pVTZ computations as the estimate for the SCF-CBS limit.

To further improve the accuracy of the interaction energies, we determined frozen-core CCSD(T) corrections for all 10178 configurations using the aug-cc-pVDZ basis set including the aforementioned bond functions. We then obtained the final interaction energies by adding to the SCF/aug-cc-pVTZ energies the extrapolated MP2 correlation energies and the differences of the CCSD(T)/aug-cc-pVDZ and MP2/aug-cc-pVDZ energies,

$$V_{\text{final}} = V_{\text{SCF}}^{\text{TZ}} + V_{\text{MP2 corr}}^{\text{CBS}} + V_{\text{CCSD(T)}}^{\text{DZ}} - V_{\text{MP2}}^{\text{DZ}}. \quad (2)$$

In order to fine tune the potential, we changed the value of  $\beta$  in Eq. (1) from 3 to 1.838, as the latter value results in the best overall agreement between calculated values for the second acoustic virial coefficient and experimentally derived values. We shall discuss the effect of the value of  $\beta$  on the PES and the calculated thermophysical property values as well as details of our fine tuning procedure in Sec. III C.

The results of the *ab initio* calculations for all 10178 configurations of two EtO molecules can be found in the supplementary material.<sup>23</sup> The CFOUR program<sup>27</sup> was used for the CCSD(T) calculations. The MP2 calculations were performed using GAUSSIAN 03.<sup>28</sup>

### C. Analytical potential function

We have fitted a site-site potential function with 19 sites per molecule to the calculated interaction energies. The sites were initially placed intuitively within each molecule as follows. There is one site for each of the seven atoms, one site for each of the four C–H bonds, two sites along each of the two C–O bonds, two sites along the C–C bond, and two sites at the positions of the free electron pairs of the oxygen atom.

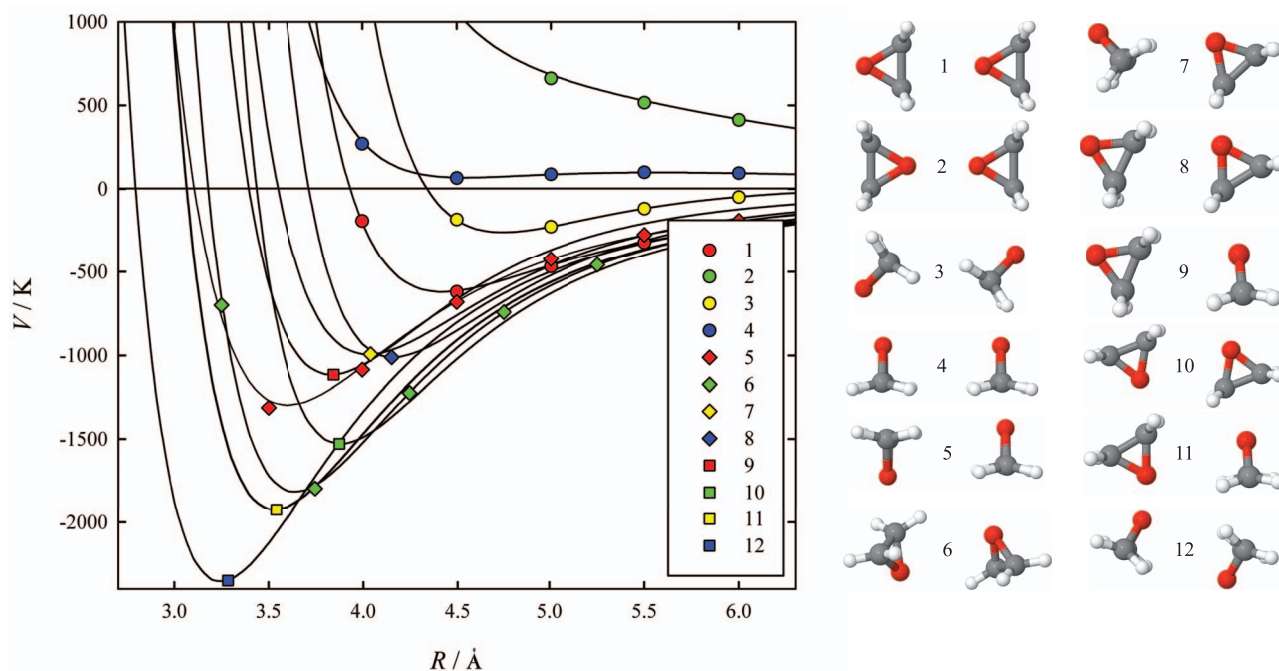


FIG. 1. Distance dependence of the EtO–EtO interaction potential for six of the 949 generated angular orientations (1–6) as well as for the angular orientations of the six equilibrium structures (7–12). The *ab initio* calculated values are represented by symbols and the fitted analytical potential function by solid lines.

The sites are arranged in accordance with the  $C_{2v}$  symmetry of EtO. This results in eight different types of sites and 36 different types of site-site combinations. The functional form used for each site-site interaction is given by

$$V(R_{ij}) = A_{ij} \exp(-\alpha_{ij} R_{ij}) - f_6(R_{ij}, b_{ij}) \frac{C_{6ij}}{R_{ij}^6} - f_8(R_{ij}, b_{ij}) \frac{C_{8ij}}{R_{ij}^8} + \frac{q_i q_j}{R_{ij}}, \quad (3)$$

where  $R_{ij}$  is the distance between site  $i$  in molecule 1 and site  $j$  in molecule 2. The damping functions  $f_6$  and  $f_8$  by Tang and Toennies<sup>29</sup> are given as

$$f_n(R_{ij}, b_{ij}) = 1 - \exp(-b_{ij} R_{ij}) \sum_{k=0}^n \frac{(b_{ij} R_{ij})^k}{k!}. \quad (4)$$

The total interaction potential is the sum over all 361 site-site interactions,

$$V(R, \theta_1, \theta_2, \psi_1, \psi_2, \phi) = \sum_{i=1}^{19} \sum_{j=1}^{19} V_{ij}[R_{ij}(R, \theta_1, \theta_2, \psi_1, \psi_2, \phi)]. \quad (5)$$

The interaction parameters  $A$ ,  $\alpha$ ,  $b$ ,  $C_6$ , and  $C_8$  for all 36 types of site-site combinations, the site charges  $q$  for all eight types of sites, and the positions of the sites within the molecule were fully optimized in a nonlinear least-squares fit to the 10178 calculated interaction energies. A visualization of the sites can be found in the supplementary material.<sup>23</sup> We gave special weight to the configurations of the six local minima. Furthermore, the only constraint was that the total charge of the monomers had to be zero.

The dipole moment of the EtO monomer calculated from the fitted site charges of 1.941 D is in reasonable agreement with the experimental value of  $(1.88 \pm 0.01)$  D<sup>22</sup> and in excellent agreement with the value of 1.945 D obtained from an *ab initio* calculation for the isolated monomer at the frozen-core CCSD(T)/aug-cc-pVQZ level. The components of the quadrupole tensor resulting from the fitted charges also agree within a few percent with the respective values from the *ab initio* calculation for the monomer. In other words, the fitted potential function predicts nearly the same values for the multipole moments as the direct *ab initio* calculation of these quantities, even though no restrictions in regard to these have been imposed during the fit. See the supplementary material<sup>23</sup> for detailed values obtained from the multipole analysis.

The highly anisotropic character of the PES is illustrated in Fig. 1, which shows the distance dependence of the fitted analytical potential function and the interaction energies from the *ab initio* calculations for selected angular configurations. Figure 2 shows the interaction energies calculated from the analytical potential function versus the *ab initio* energies up to 2500 K. The small deviations from a straight line demonstrate the high quality of the fit. Towards the highly repulsive region the quality of the fit decreases. However, this is of negligible effect for the calculation of thermophysical properties of ethylene oxide for temperatures below 1000 K.

The analytical potential function exhibits six distinct equilibrium structures with interaction energies of  $-2357.0$  K,  $-1926.4$  K,  $-1529.0$  K,  $-1116.1$  K,  $-1012.6$  K, and  $-995.2$  K, which are also displayed in Fig. 1. The parameters as well as a Fortran 90 routine of the potential function and details about the equilibrium configurations are provided in the supplementary material.<sup>23</sup> There we also provide a study of the influence of different levels of theory and basis sets on the minimum energies.

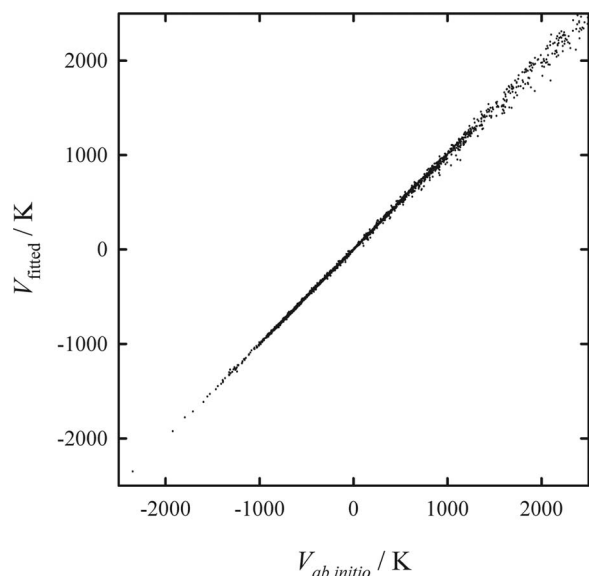


FIG. 2. Interaction energies from the analytical fit as given by Eq. (5) versus *ab initio* calculated interaction energies from Eq. (2).

### III. SECOND VIRIAL COEFFICIENTS

#### A. Theory

The classical second virial coefficient for a gas composed of rigid molecules is given by

$$B_{\text{cl}}(T) = -\frac{N_{\text{A}}}{2} \int_0^{\infty} \langle f_{12} \rangle_{\Omega_1, \Omega_2} d\mathbf{R}, \quad (6)$$

with

$$f_{12} = \exp \left[ -\frac{V(\mathbf{R}, \Omega_1, \Omega_2)}{k_{\text{B}}T} \right] - 1, \quad (7)$$

where  $\mathbf{R}$  is the distance vector connecting the centers of mass of the two molecules and  $\Omega_1$  and  $\Omega_2$  represent the angular orientations of molecules 1 and 2, respectively. The angle brackets denote an average over these angular orientations. At low and moderate temperatures, the classical treatment is insufficient and quantum effects have to be accounted for. This is achieved by substituting the pair potential  $V$  in Eq. (7) by the quadratic Feynman-Hibbs effective pair potential.<sup>11</sup> In the case of two identical asymmetric tops, the effective potential can be written as

$$V_{\text{QFH}}(T) = V + \frac{\hbar^2}{12k_{\text{B}}T} \left[ \frac{1}{m} \left( \frac{\partial^2 V}{\partial x^2} + \frac{\partial^2 V}{\partial y^2} + \frac{\partial^2 V}{\partial z^2} \right) + \frac{1}{2} \sum_{n=1}^2 \left( \frac{1}{I_a} \frac{\partial^2 V}{\partial \psi_{a,n}^2} + \frac{1}{I_b} \frac{\partial^2 V}{\partial \psi_{b,n}^2} + \frac{1}{I_c} \frac{\partial^2 V}{\partial \psi_{c,n}^2} \right) \right], \quad (8)$$

where  $m$  is the molecular mass;  $x$ ,  $y$ , and  $z$  are the cartesian components of  $\mathbf{R}$ ;  $I_a$ ,  $I_b$ , and  $I_c$  are the moments of inertia for the principal axes  $a$ ,  $b$ , and  $c$ . The angles  $\psi_{a,n}$ ,  $\psi_{b,n}$ , and  $\psi_{c,n}$  correspond to rotations of the  $n$ th molecule around its principal axes.

Once the second virial coefficient as a function of temperature is known, the second acoustic virial coefficient can

be calculated using the relation

$$\beta_{\text{a}}(T) = 2 \left[ B(T) + (\gamma^0 - 1)T \frac{dB(T)}{dT} + \frac{(\gamma^0 - 1)^2}{2\gamma^0} T^2 \frac{d^2 B(T)}{dT^2} \right], \quad (9)$$

where  $\gamma^0 = C_p^0/C_V^0$  is the ratio of the isochoric and isobaric heat capacities in the ideal-gas limit.

#### B. Numerical evaluation

We evaluated the integral for the second virial coefficient as given by Eq. (6) numerically using the Mayer-sampling Monte Carlo approach proposed by Singh and Kofke.<sup>30</sup> This method involves a biased two-particle Monte Carlo simulation using importance sampling. The sampling distribution  $\pi$  is chosen to be equal to the absolute value of the integrand  $\tilde{B}$  of the virial coefficient  $B$ ,  $\pi = |\tilde{B}|$ . Trial moves are accepted with a probability of  $\min(1, \pi_{\text{new}}/\pi_{\text{old}})$ . The value of the second virial coefficient is given by

$$B(T) = B_{\text{hs}} \frac{\langle \tilde{B}(T)/\pi \rangle_{\pi}}{\langle \tilde{B}_{\text{hs}}/\pi \rangle_{\pi}}. \quad (10)$$

Here, the hard-sphere fluid serves as the reference system as indicated by the subscript *hs*. The angle brackets denote the weighted simulation averages. Results for multiple temperatures can be calculated in a single simulation.<sup>30,31</sup> This is done by simply calculating the integrand of the virial coefficient for all considered temperatures at each simulation step, while the sampling distribution is chosen to be the integrand of the virial coefficient at a fixed sampling temperature  $T_s$ . In our experience, choosing the lowest considered temperature as the sampling temperature usually yields the best results.

The second virial coefficient was calculated for 65 temperatures ranging from 220 K up to 1000 K using a sampling temperature of  $T_s = 220$  K. Data from 16 independent simulation runs, each with  $10^{11}$  trial moves, were averaged to give the final results.

To obtain the second acoustic virial coefficient, we fitted a polynomial, see Eq. (11), to the computed values of the second virial coefficient in order to determine the first and second temperature derivatives in Eq. (9). For  $C_p^0(T)$  we used the data of Chao *et al.*<sup>32</sup> These values are in good agreement with data of Hurly<sup>33</sup> in the range of 285 K–440 K from speed of sound measurements with a maximum deviation between the two sources of 0.08% at around 310 K. Quantum effects account for a noticeable contribution to the values of the second virial coefficient, especially at lower temperatures. At room temperature, they account for approximately  $8 \text{ cm}^3 \text{ mol}^{-1}$ . We give detailed values for the contribution due to the quantum effects resulting from Eq. (8) in the supplementary material.<sup>23</sup>

#### C. Fine tuning of the PES and results

Before we discuss our results we have to take a closer look at the fine tuning procedure of the PES. As mentioned in Sec. II B the calculated *ab initio* energies were extrapolated using the scheme suggested by Halkier *et al.*<sup>26</sup> We used that

scheme to generate two sets of extrapolated energies, which resulted in two distinct fits for the potential function,  $V_A$  and  $V_B$ . The first one,  $V_A$ , aims to agree with the values for the second acoustic virial coefficient determined by Hurly<sup>33</sup> from speed of sound measurements within the stated error bounds. Particularly at higher temperatures the given uncertainties are relatively small.  $V_B$  on the other hand follows the values for the second virial coefficient derived by Hurly<sup>33</sup> from his values for the second acoustic virial coefficient, for which he used a simple hard-core Lennard-Jones (HCLJ) potential. In an iterative procedure, we chose a coefficient  $\beta$  and evaluated the *ab initio* interaction energies according to Eqs. (1) and (2). We then fitted the potential function and used it to calculate the virial coefficients as described in Sec. III B. The resulting values for  $\beta$  are 1.8380 and 2.2225 for  $V_A$  and  $V_B$ , respectively.

For both the second virial coefficients and second acoustic virial coefficients, the values obtained from  $V_B$  and those obtained from Hurly's<sup>33</sup> HCLJ potential are in very good agreement for all temperatures. However, above 340 K the values for the second acoustic virial coefficient for both  $V_B$  and HCLJ lie above the relatively tight error range that Hurly gave for these temperatures. Hence, it appears that Hurly gave a different weight to his experimental values than we did. It should be mentioned that uncertainties in  $C_p^0$  alone cannot account for this. We conservatively estimated the error in  $\beta_a$  resulting from uncertainties in  $C_p^0$  to be  $\pm 2 \text{ cm}^3 \text{ mol}^{-1}$  by propagating the maximum deviation between the most reliable sources<sup>32-34</sup> for  $C_p^0$  using Eq. (9). The maximum deviation to be found in  $C_p^0$  in the interval of 285 K to 440 K occurs at 340 K with 0.047  $R$ , which translates into  $1.7 \text{ cm}^3 \text{ mol}^{-1}$  at 285 K and into  $0.6 \text{ cm}^3 \text{ mol}^{-1}$  at 440 K.

Based on our observations we chose the values for the second virial coefficients and second acoustic virial coefficients resulting from  $V_B$  as a conservative upper error bound to the values calculated on the basis of  $V_A$ . We assumed the lower margin of error to be of the same magnitude.

The results for the second acoustic virial coefficient are displayed in Fig. 3, and those for the second virial coefficient are shown in Fig. 4. We are confident that the potential function  $V_A$  is a good approximation to the true pair potential as we have managed to stay almost entirely within the error bounds of Hurly's<sup>33</sup> experimental data for the second acoustic virial coefficient.

To our knowledge, Stryjek<sup>35</sup> provided the only data set for the second virial coefficient determined from experiment. While Stryjek's values obviously follow a different temperature trend than our and Hurly's<sup>33</sup> values, we are still within Stryjek's error range of  $\pm 35 \text{ cm}^3 \text{ mol}^{-1}$ . We also extracted values for the second virial coefficient from the isothermal data of Walters and Smith<sup>36</sup> from plots of  $(Z - 1)/\rho$  vs.  $\rho$ . We give our resulting values as they are and without an uncertainty estimate.

The virial coefficients resulting from  $V_A$  and  $V_B$  were fitted using the following polynomial formula:

$$B(T) = \sum_{k=-1}^5 c_k (T^*)^{-k} + c_{10} (T^*)^{-10}, \quad (11)$$

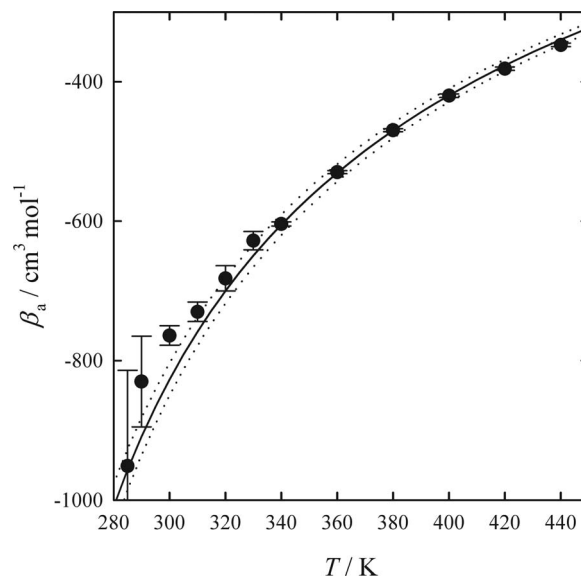


FIG. 3. Second acoustic virial coefficient for ethylene oxide as a function of temperature: —, calculated values from potential function  $V_A$ ; ···, confidence interval determined by  $V_B$ ; •, Hurly (Ref. 33).

where  $T^* = T/(100 \text{ K})$ . The input data for the fit were weighted with the squared inverse of the 67% confidence limits resulting from the independent simulation runs. The coefficients in Eq. (11) for both potentials as well as the input data and the values resulting from the fits are given in the supplementary material.<sup>23</sup>

#### IV. TRANSPORT PROPERTIES

A further validation of the quality of our proposed pair potential function can be obtained from a comparison between calculated and experimentally determined transport

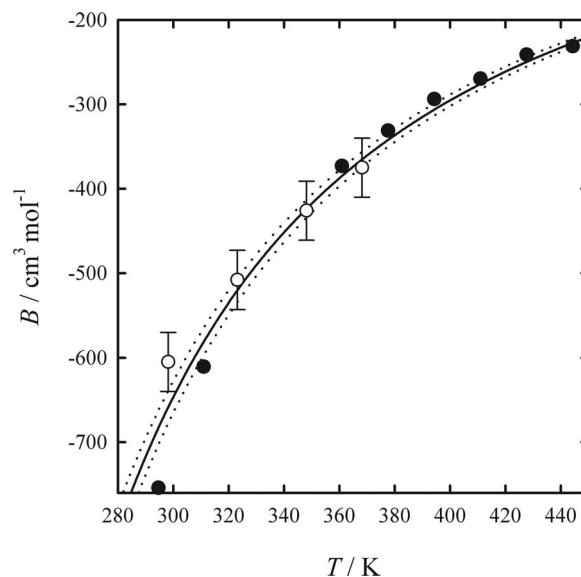


FIG. 4. Second virial coefficient for ethylene oxide as a function of temperature: —, calculated from potential function  $V_A$ ; ···, confidence interval determined by  $V_B$ ; ○, Stryjek (Ref. 35); •, values extracted from the isotherms of Walters and Smith (Ref. 36). Hurly's values (Ref. 33), which are based on his HCLJ potential, would be indistinguishable from the upper confidence curve on this scale.

property data in the dilute-gas limit. For ethylene oxide, the available data are scant. To our knowledge, there exist only four published data sets for thermal conductivity<sup>37–40</sup> from experiment and only a single datum<sup>37</sup> for shear viscosity deduced through similitude theory from one of the aforementioned thermal conductivity measurements.

## A. Theory

The transport properties of a dilute gas can be calculated using the kinetic theory of molecular gases.<sup>12</sup> The shear viscosity  $\eta$  of a pure gas is given by

$$\eta = \frac{k_B T}{\langle v \rangle_0} \frac{f_\eta^{(n)}}{\mathfrak{S}(2000)}, \quad (12)$$

where  $\langle v \rangle_0 = 4(k_B T / \pi m)^{1/2}$  is the average relative thermal speed, and  $\mathfrak{S}(2000)$  is a temperature-dependent generalized cross section. The notation and conventions employed are given elsewhere.<sup>12,42,43</sup> The quantity  $f_\eta^{(n)}$  is an  $n$ th-order correction factor. It accounts for higher basis function terms in the perturbation series expansion of the solution of the Boltzmann equation<sup>12</sup> and can be written as

$$f_\eta^{(n)} = \mathfrak{S}(2000) \frac{S_{11}^{(n)}}{S^{(n)}}, \quad (13)$$

where  $S^{(n)}$  is a determinant of cross sections and  $S_{11}^{(n)}$  its minor. In the second-order approximation, which results from including the basis functions  $\Phi^{2000}$ ,  $\Phi^{2010}$ ,  $\Phi^{2001}$ , and  $\Phi^{0200}$ , we have<sup>42,44</sup>

$$S^{(2)} = \begin{vmatrix} \mathfrak{S}(2000) & \mathfrak{S}\begin{pmatrix} 2000 \\ 2010 \end{pmatrix} & \mathfrak{S}\begin{pmatrix} 2000 \\ 2001 \end{pmatrix} & \mathfrak{S}\begin{pmatrix} 2000 \\ 0200 \end{pmatrix} \\ \mathfrak{S}\begin{pmatrix} 2010 \\ 2000 \end{pmatrix} & \mathfrak{S}(2010) & \mathfrak{S}\begin{pmatrix} 2010 \\ 2001 \end{pmatrix} & \mathfrak{S}\begin{pmatrix} 2010 \\ 0200 \end{pmatrix} \\ \mathfrak{S}\begin{pmatrix} 2001 \\ 2000 \end{pmatrix} & \mathfrak{S}\begin{pmatrix} 2001 \\ 2010 \end{pmatrix} & \mathfrak{S}(2001) & \mathfrak{S}\begin{pmatrix} 2001 \\ 0200 \end{pmatrix} \\ \mathfrak{S}\begin{pmatrix} 0200 \\ 2000 \end{pmatrix} & \mathfrak{S}\begin{pmatrix} 0200 \\ 2010 \end{pmatrix} & \mathfrak{S}\begin{pmatrix} 0200 \\ 2001 \end{pmatrix} & \mathfrak{S}(0200) \end{vmatrix}. \quad (14)$$

In the present paper, we used a third-order approximation that includes the basis functions  $\Phi^{2000}$ ,  $\Phi^{2010}$ ,  $\Phi^{2001}$ ,  $\Phi^{0200}$ ,  $\Phi^{2020}$ ,  $\Phi^{2011}$ ,  $\Phi^{2002}$ ,  $\Phi_2^{2100}$ , and  $\Phi_2^{2200}$ . The structure of the resulting  $9 \times 9$  determinant  $S^{(3)}$  is similar to  $S^{(2)}$ .

For a pure gas consisting of rigid-rotor (rr) molecules, the thermal conductivity  $\lambda$  can be written as

$$\lambda_{\text{rr}} = \frac{5k_B^2 T}{2m\langle v \rangle_0} \left[ \frac{S_{11}^{(1)} - rS_{21}^{(1)}}{S^{(1)}} + \frac{r^2 S_{22}^{(1)} - rS_{12}^{(1)}}{S^{(1)}} \right] f_{\lambda_{\text{rr}}}^{(n)}, \quad (15)$$

with

$$S^{(1)} = \begin{vmatrix} \mathfrak{S}(1010)_{\text{rr}} & \mathfrak{S}\begin{pmatrix} 1010 \\ 1001 \end{pmatrix}_{\text{rr}} \\ \mathfrak{S}\begin{pmatrix} 1001 \\ 1010 \end{pmatrix}_{\text{rr}} & \mathfrak{S}(1001)_{\text{rr}} \end{vmatrix}. \quad (16)$$

The parameter  $r$  is given by

$$r = \left( \frac{2 C_{\text{rot}}^0}{5 k_B} \right)^{1/2}, \quad (17)$$

where for an asymmetric top  $C_{\text{rot}}^0 = 3k_B/2$ . For real molecular gases, the thermal conductivity also includes contributions from the transport of vibrational energy, which are neglected in the rigid-rotor approximation. Assuming that the vibrational states of the molecules do not change during a collision and that the influence of the vibrational motion on the trajectories is negligible, it can be shown<sup>43</sup> that the contribution of vibrational energy transport to the thermal conductivity is a simple additive correction,<sup>43,45,46</sup>

$$\lambda = \lambda_{\text{rr}} + \frac{C_{\text{vib}}^0}{m} \mathcal{D}_{\text{self,rr}}, \quad (18)$$

where  $\mathcal{D}_{\text{self,rr}}$  is the product of mass density and self-diffusion coefficient within the rigid-rotor approximation,

$$\mathcal{D}_{\text{self,rr}} = \rho D_{\text{self,rr}} = \frac{k_B T}{\langle v \rangle_0} \frac{f_{\mathcal{D}_{\text{self,rr}}}^{(n)}}{\sigma'(1000)_{\text{rr}}}. \quad (19)$$

Equation (18) was first proposed by Liang and Tsai<sup>45,46</sup> for determining the thermal conductivity of polyatomic fluids from molecular dynamics simulations. In the present work, we evaluated  $\lambda_{\text{rr}}$  and  $\mathcal{D}_{\text{self,rr}}$  using the second-order kinetic theory expressions given in Ref. 43. For  $C_{\text{vib}}^0$ , we used values derived from the equation for  $C_V^0$  given in Ref. 32.

## B. Numerical evaluation of the generalized cross sections

We computed the generalized cross sections needed to evaluate the transport properties by means of classical trajectories using an extended version of the TRAJECT software code.<sup>14,15</sup> For a given total energy,  $E = E_{\text{tr}} + E_{\text{rot}}$ , classical trajectories describing collisions of two rigid EtO molecules were obtained by integrating Hamilton's equations for asymmetric tops from pre- to post-collisional values with an initial and final separation of 1000 Å. Total-energy-dependent generalized cross sections, which are 13-dimensional integrals over the initial states, were calculated for 25 values of  $E$  from 100 K to 20 000 K by means of a simple Monte Carlo procedure utilizing quasi-random numbers. Up to 800 000 trajectories were computed for each total energy value. For low energies, the number of trajectories had to be reduced significantly, because the computational demand to achieve a sufficient accuracy for a particular trajectory increases as the energy decreases. The final integration over  $E$  to obtain the temperature-dependent generalized cross sections was performed using Chebyshev quadrature.

The uncertainty of the calculated values for the shear viscosity and the self-diffusion coefficient is about 2% for the potential function  $V_A$ . This estimate takes into account the precision of the calculated cross sections, uncertainties due to the potential function (differences of the transport property values resulting from  $V_A$  and  $V_B$ ), and possible deficiencies of the rigid-rotor approximation (estimated to be 1%). For the thermal conductivity, the uncertainties of the  $C_{\text{vib}}^0$  values, which we estimated from the differences between  $C_V^0$  in a similar manner as we have done for the second acoustic virial coefficient, have to be taken into account as well. The resulting estimate for the uncertainty of our thermal conductivity values is 3%. Quantum corrections to the transport properties should be

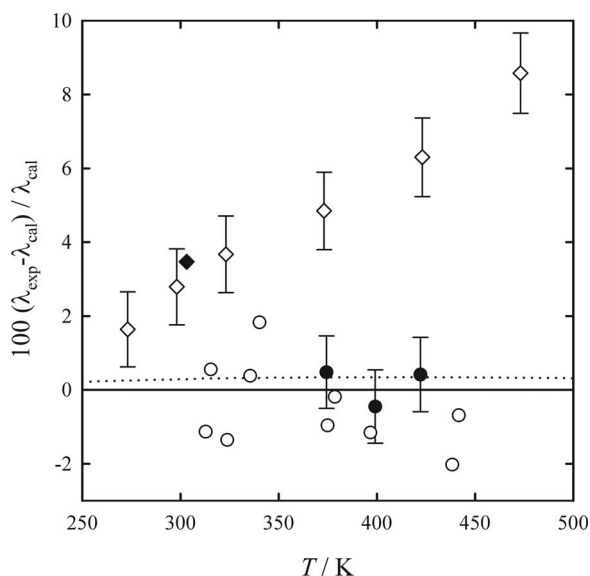


FIG. 5. Relative deviations of thermal conductivity values in the dilute-gas limit from results for the potential function  $V_A$ :  $\blacklozenge$ , Senftleben (Ref. 37);  $\bullet$ , Vines and Bennett (Ref. 38);  $\circ$ , El Nadi and Salam (Ref. 39);  $\diamond$ , Senftleben (Ref. 40);  $\cdots$ , results for potential function  $V_B$ .

negligibly small for ethylene oxide. Even for water vapor, for which the quantum corrections to the classical second virial coefficient are huge,<sup>18</sup> the classical trajectory approach yields viscosity<sup>47</sup> and thermal conductivity<sup>43</sup> values that are in excellent agreement with the best experimental data.

Our calculated values for shear viscosity, thermal conductivity, and the product of self-diffusion coefficient with mass density in the temperature range of 200 K to 1000 K are given in the supplementary material.<sup>23</sup>

### C. Results

A critical review of literature has yielded only four sets of experimental data for the thermal conductivity of ethylene oxide.<sup>37–40</sup> We compare those values with our own in Fig. 5. All of the experiments were conducted in the 1950s and 1960s and no further work on this subject has been published since.

In 1953, Senftleben<sup>37</sup> determined a low pressure value for the thermal conductivity of ethylene oxide at 30 °C. His datum exceeds our calculated value by 3.4%. A year later in 1954 Vines and Bennett<sup>38</sup> used a hot wire apparatus to measure the thermal conductivity at pressures up to 1 bar at three temperatures between 100 °C and 150 °C. They extrapolated their results to the dilute-gas limit. Those values are in very good agreement with our calculations and deviate not more than 1% from them. A hot wire device was also used in 1960 by El Nadi and Salam<sup>39</sup> for measurements at pressures between 2 Torr and 760 Torr and temperatures of 40 °C to 170 °C. Their values for the thermal conductivity in the dilute-gas limit generally agree with our computed values within  $\pm 2\%$ .

In 1964, Senftleben once more published data<sup>40</sup> on the thermal conductivity of ethylene oxide at low pressure, this time in a large temperature range between 0 °C and 400 °C. In Ref. 48, Senftleben describes the hot wire method used by him to obtain these data. He states that the temperature dif-

ferences between the heated wire and the surrounding wall range from 50 K to 200 K. The values given in his paper are derived from a polynomial fit to his primary data for the thermal conductivity with respect to the temperature. From that function values given for temperatures greater than 200 °C were extrapolated. Based on this information it is our opinion that the values of the thermal conductivity as determined and published by Senftleben<sup>40</sup> are of questionable accuracy. The deviations of Senftleben's values from our values increase progressively with temperature and reach +23% at 673.15 K. In Fig. 5, we have omitted those values with deviations larger than 10%. Senftleben<sup>40</sup> conducted his measurements using carbon dioxide as reference. We attempted to correct the thermal conductivity values for ethylene oxide using the most recent thermal conductivity values<sup>49</sup> for carbon dioxide. Senftleben's<sup>40</sup> CO<sub>2</sub> data are in good agreement up to 423 K, and only values from 473 K and higher were significantly affected by our correction attempt, e.g., the value at 673.15 K would deviate only +15%. It is our opinion that other sources of systematic error exist in his measurements on ethylene oxide, and we suspect a general invalidity of his extrapolations at temperatures larger than 200 °C. We have not only included Senftleben's results in our comparison merely for the purpose of completeness, but to emphasize using caution when using those data, which have influenced correlations for industry, see, for example, Ref. 41.

Furthermore, in Fig. 5 we show the results for the thermal conductivity for ethylene oxide using the potential  $V_B$  for the calculations. The maximum deviation is about +0.35% at a temperature of 400 K.

Our literature review yielded a single datum<sup>37</sup> for the viscosity of ethylene oxide vapor. This datum does not result from a direct measurement, as it has been derived by Senftleben using similitude theory from the thermal conductivity value that he determined in his 1953 work.<sup>37</sup> That value deviates from our computed value by +1.9%.

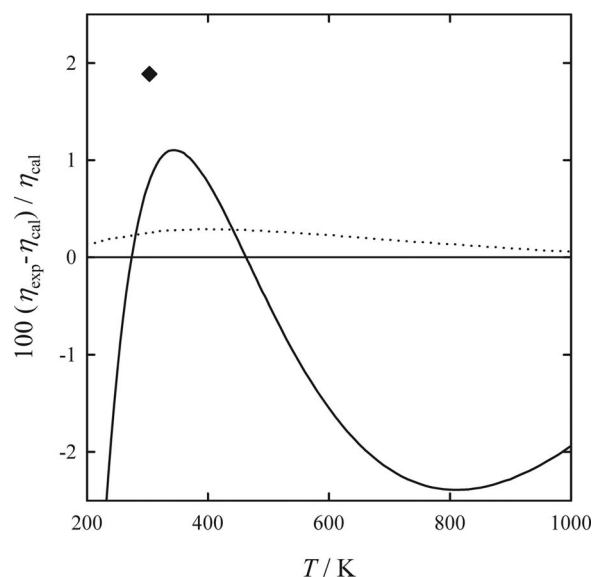


FIG. 6. Relative deviations of shear viscosity values in the dilute-gas limit from results for the potential function  $V_A$ :  $\blacklozenge$ , Senftleben (Ref. 37);  $\text{—}$ , corresponding state: Stiel and Thodos correlation as given by Ref. 41;  $\cdots$ , results for potential function  $V_B$ .

For lack of any further experimental data, we also include the results for shear viscosity as calculated from the Stiel and Thodos correlation according to Ref. 41, which is based on a corresponding states principle. We give a graphical comparison in Fig. 6. From the experience we gained in our previous works, we know that the quality of the results in thermal conductivity is reflected in the quality of the results for viscosity and vice versa. Therefore, we are confident that the viscosity data we present in this work will be supported by future experimental measurements.

It is notable that the effect on the calculated thermal conductivity and viscosity values from using a potential function resulting from a different extrapolation, i.e.,  $V_B$  vs.  $V_A$ , is quite small and well within our stated uncertainties. This further corroborates that our approach is justified and that our suggested potential function is well suited to determine transport properties.

There appear to be no experimental data for the self-diffusion coefficient of gaseous ethylene oxide.

## V. SUMMARY AND CONCLUSIONS

We have determined a new six-dimensional intermolecular potential energy surface for two rigid ethylene oxide molecules from quantum-chemical *ab initio* calculations. The interaction energies were calculated for 10178 distinct configurations at the MP2 level of theory using the aug-cc-pVDZ and aug-cc-pVTZ basis sets and extrapolated to the complete basis set limit. Furthermore, coupled-cluster corrections were determined at the CCSD(T)/aug-cc-pVDZ level. In all calculations, the basis sets were supplemented by a small set of bond functions located midway between the two molecules.

A 19-center site-site potential function was then fitted to the computed interaction energies. Using accurate experimental data for the second acoustic virial coefficient as guidance, the basis set extrapolation scheme for the interaction energies was slightly modified by adjusting the value of a single parameter.

To validate the resulting potential function, we have calculated values for the second virial coefficient as well as for shear viscosity and thermal conductivity in the dilute-gas limit for temperatures ranging from 200 K to 1000 K. The effect of the fine tuning of the potential function on the values of the transport properties lies well within our estimated uncertainties for these quantities, thereby corroborating our approach. Our values for the second virial coefficient generally agree with the few experimental data. The calculated values for thermal conductivity are in good agreement with the best available data. For shear viscosity, there are insufficient experimental data to allow for a meaningful comparison. However, they are supported by a single datum obtained through similitude theory as well as a corresponding state correlation. It is also our past experience that our methodology usually gives results of consistent quality for thermal conductivity and shear viscosity. The lack of reliable thermophysical property data for ethylene oxide indicates that our calculated values are currently the most accurate estimates for the thermophysical properties of ethylene oxide vapor.

## ACKNOWLEDGMENTS

We wish to acknowledge the financial support by the Deutsche Forschungsgemeinschaft (DFG), Grant No. BI 1389/3-1.

- <sup>1</sup>P. Dutia, Chem. Weekly 199 (26 January 2010).
- <sup>2</sup>“4th Challenge of the Industrial Fluid Properties Simulation Collective,” see <http://fluidproperties.org>.
- <sup>3</sup>R. D. Mountain, *Fluid Phase Equilib.* **274**, 1 (2008).
- <sup>4</sup>F. H. Case, J. Brennan, A. Chaka, K. D. Dobbs, D. G. Friend, P. A. Gordon, J. D. Moore, R. D. Mountain, J. D. Olson, R. B. Ross, M. Schiller, V. K. Shen, and E. A. Stahlberg, *Fluid Phase Equilib.* **274**, 2 (2008).
- <sup>5</sup>J. D. Olson and L. C. Wilson, *Fluid Phase Equilib.* **274**, 10 (2008).
- <sup>6</sup>B. Eckl, J. Vrabec, and H. Hasse, *Fluid Phase Equilib.* **274**, 16 (2008).
- <sup>7</sup>T. J. Müller, S. Roy, W. Zhao, A. Maaß, and D. Reith, *Fluid Phase Equilib.* **274**, 27 (2008).
- <sup>8</sup>X. Li, L. Zhao, T. Cheng, L. Liu, and H. Sun, *Fluid Phase Equilib.* **274**, 36 (2008).
- <sup>9</sup>M. H. Ketko, J. Rafferty, J. I. Siepmann, and J. J. Potoff, *Fluid Phase Equilib.* **274**, 44 (2008).
- <sup>10</sup>K. Raghavachari, G. W. Trucks, J. A. Pople, and M. Head-Gordon, *Chem. Phys. Lett.* **157**, 479 (1989).
- <sup>11</sup>R. P. Feynman and A. R. Hibbs, *Quantum Mechanics and Path Integrals* (McGraw-Hill, New York, 1965).
- <sup>12</sup>F. R. W. McCourt, J. J. M. Beenakker, W. E. Köhler, and I. Kuščer, *Nonequilibrium Phenomena in Polyatomic Gases*, Vol. I: Dilute Gases (Clarendon Press, Oxford, 1990).
- <sup>13</sup>C. F. Curtiss, *J. Chem. Phys.* **75**, 1341 (1981).
- <sup>14</sup>E. L. Heck and A. S. Dickinson, *Comput. Phys. Commun.* **95**, 190 (1996).
- <sup>15</sup>A. S. Dickinson, R. Hellmann, E. Bich, and E. Vogel, *Phys. Chem. Chem. Phys.* **9**, 2836 (2007).
- <sup>16</sup>E. M. Mas and K. Szalewicz, *J. Chem. Phys.* **104**, 7606 (1996).
- <sup>17</sup>M. Jeziorska, P. Jankowski, K. Szalewicz, and B. Jeziorski, *J. Chem. Phys.* **113**, 2957 (2000).
- <sup>18</sup>R. Bukowski, K. Szalewicz, G. C. Groenenboom, and A. van der Avoird, *J. Chem. Phys.* **128**, 094313 (2008).
- <sup>19</sup>R. Hellmann, E. Bich, and E. Vogel, *J. Chem. Phys.* **128**, 214303 (2008).
- <sup>20</sup>K. A. Peterson and T. H. Dunning, Jr., *J. Chem. Phys.* **117**, 10548 (2002).
- <sup>21</sup>L. A. Evseeva and L. M. Sverdlov, *Sov. Phys. J.* **11**, 70 (1968).
- <sup>22</sup>G. L. Cunningham, Jr., A. W. Boyd, R. J. Myers, W. D. Gwinn, and W. I. L. Van, *J. Chem. Phys.* **19**, 676 (1951).
- <sup>23</sup>See supplementary material at <http://dx.doi.org/10.1063/1.4899074> for details of Euler-angles and rotation matrices used; parameters, the equilibrium structures, and a Fortran 90 routine of the analytical potential function; visualizations of the interaction sites; details of multipole moment analysis; results of the *ab initio* calculations for all 10178 points used for the fit of the analytical potential function; tables of all thermophysical property values calculated in this work.
- <sup>24</sup>S. F. Boys and F. Bernardi, *Mol. Phys.* **19**, 553 (1970).
- <sup>25</sup>R. A. Kendall, T. H. Dunning, Jr., and R. J. Harrison, *J. Chem. Phys.* **96**, 6796 (1992).
- <sup>26</sup>A. Halkier, T. Helgaker, P. Jørgensen, W. Klopper, H. Koch, J. Olsen, and A. K. Wilson, *Chem. Phys. Lett.* **286**, 243 (1998).
- <sup>27</sup>CFour, coupled-cluster techniques for computational chemistry, a quantum-chemical program package by J. F. Stanton, J. Gauss, M. E. Harding, P. G. Szalay with contributions from A. A. Auer, R. J. Bartlett, U. Benedikt, C. Berger, D. E. Bernholdt, Y. J. Bomble, O. Christiansen, M. Heckert, O. Heun, C. Huber, T.-C. Jagau, D. Jonsson, J. Jusélius, K. Klein, W. J. Lauderdale, D. A. Matthews, T. Metzroth, D. P. O'Neill, D. R. Price, E. Prochnow, K. Ruud, F. Schiffmann, S. Stopkovicz, A. Tajti, J. Vázquez, F. Wang, J. D. Watts and the integral packages MOLECULE (J. Almlöf and P. R. Taylor), PROPS (P. R. Taylor), ABACUS (T. Helgaker, H. J. Aa. Jensen, P. Jørgensen, and J. Olsen), and ECP routines by A. V. Mitin and C. van Wüllen, For the current version, see <http://www.cfour.de>.
- <sup>28</sup>M. J. Frisch, G. W. Trucks, H. B. Schlegel, G. E. Scuseria, M. A. Robb, J. R. Cheeseman, J. A. Montgomery, Jr., T. Vreven, K. N. Kudin, J. C. Burant, J. M. Millam, S. S. Iyengar, J. Tomasi, V. Barone, B. Mennucci, M. Cossi, G. Scalmani, N. Rega, G. A. Petersson, H. Nakatsuji, M. Hada, M. Ehara, K. Toyota, R. Fukuda, J. Hasegawa, M. Ishida, T. Nakajima, Y. Honda, O. Kitao, H. Nakai, M. Klene, X. Li, J. E. Knox, H. P. Hratchian, J. B. Cross, V. Bakken, C. Adamo, J. Jaramillo, R. Gomperts, R. E. Stratmann, O. Yazyev, A. J. Austin, R. Cammi, C. Pomelli, J. W. Ochterski, P. Y. Ayala,

- K. Morokuma, G. A. Voth, P. Salvador, J. J. Dannenberg, V. G. Zakrzewski, S. Dapprich, A. D. Daniels, M. C. Strain, O. Farkas, D. K. Malick, A. D. Rabuck, K. Raghavachari, J. B. Foresman, J. V. Ortiz, Q. Cui, A. G. Baboul, S. Clifford, J. Cioslowski, B. B. Stefanov, G. Liu, A. Liashenko, P. Piskorz, I. Komaromi, R. L. Martin, D. J. Fox, T. Keith, M. A. Al-Laham, C. Y. Peng, A. Nanayakkara, M. Challacombe, P. M. W. Gill, B. Johnson, W. Chen, M. W. Wong, C. Gonzalez, and J. A. Pople, Gaussian 03, Revision E.01, Gaussian, Inc., Wallingford, CT, 2004.
- <sup>29</sup>K. T. Tang and J. P. Toennies, *J. Chem. Phys.* **80**, 3726 (1984).
- <sup>30</sup>J. K. Singh and D. A. Kofke, *Phys. Rev. Lett.* **92**, 220601 (2004).
- <sup>31</sup>B. Jäger, R. Hellmann, E. Bich, and E. Vogel, *J. Chem. Phys.* **135**, 084308 (2011).
- <sup>32</sup>J. Chao, K. R. Hall, K. N. Marsh, and R. C. Wilhoit, *J. Phys. Chem. Ref. Data* **15**, 1369 (1986).
- <sup>33</sup>J. J. Hurly, *Int. J. Thermophys.* **23**, 667 (2002).
- <sup>34</sup>D. R. Burgess, "Thermochemical data," in *NIST Chemistry WebBook*, NIST Standard Reference Database Number 69, edited by P. J. Linstrom and W. G. Mallard (National Institute of Standards and Technology, Gaithersburg, MD, 2012), see <http://webbook.nist.gov>.
- <sup>35</sup>R. Stryjek, *Bull. Acad. Pol. Sci. Ser. Sci. Chim.* **14**, 307 (1966).
- <sup>36</sup>C. J. Walters and J. M. Smith, *Chem. Eng. Prog.* **48**, 337 (1952).
- <sup>37</sup>H. Senftleben, *Z. Angew. Phys.* **5**, 33 (1953).
- <sup>38</sup>R. G. Vines and L. A. Bennett, *J. Chem. Phys.* **22**, 360 (1954).
- <sup>39</sup>M. El Nadi and E. Salam, *Z. Phys. Chem. (Leipzig)* **215**, 121 (1960).
- <sup>40</sup>H. Senftleben, *Z. Angew. Phys.* **17**, 86 (1964).
- <sup>41</sup>C. L. Yaws, *Physical Properties: A Guide to the Physical, Thermodynamic and Transport Property Data of Industrially Important Chemical Compounds* (McGraw-Hill, New York, 1977).
- <sup>42</sup>R. Hellmann, E. Bich, E. Vogel, A. S. Dickinson, and V. Vesovic, *J. Chem. Phys.* **129**, 064302 (2008).
- <sup>43</sup>R. Hellmann and E. Bich, "An improved kinetic theory approach for calculating the thermal conductivity of polyatomic gases," *Mol. Phys.* (published online).
- <sup>44</sup>E. L. Heck and A. S. Dickinson, *Physica A* **217**, 107 (1995).
- <sup>45</sup>Z. Liang and H.-L. Tsai, *Fluid Phase Equilib.* **297**, 40 (2010).
- <sup>46</sup>Z. Liang and H.-L. Tsai, *Mol. Phys.* **108**, 1707 (2010).
- <sup>47</sup>R. Hellmann, E. Bich, E. Vogel, A. S. Dickinson, and V. Vesovic, *J. Chem. Phys.* **131**, 014303 (2009).
- <sup>48</sup>H. Senftleben, *Z. Angew. Phys.* **16**, 111 (1963).
- <sup>49</sup>R. Hellmann, *Chem. Phys. Lett.* **613**, 133 (2014).